sensors

MDPI

Communication

Optical Temperature Sensor Based on Polysilicon Waveguides

Xinru Xu [1], Yuexin Yin [1], Chunlei Sun [2,3], Lan Li [2,3], Hongtao Lin [4], Bo Tang [5], Peng Zhang [5], Changming Chen [1] and Daming Zhang [1,*]

[1] State Key Laboratory of Integrated Optoelectronics, College of Electronic Science and Engineering, Jilin University, Changchun 130012, China
[2] Key Laboratory of 3D Micro/Nano Fabrication and Characterization of Zhejiang Province, School of Engineering, Westlake University, Hangzhou 310024, China
[3] Institute of Advanced Technology, Westlake Institute for Advanced Study, Hangzhou 310024, China
[4] State Key Laboratory of Modern Optical Instrumentation, College of Information Science and Electronic Engineering, Zhejiang University, Hangzhou 310027, China
[5] Institute of Microelectronics of the Chinese Academy of Sciences, Beijing 100029, China
* Correspondence: zhangdm@jlu.edu.cn

Abstract: Traditional temperature detection has limitations in terms of sensing accuracy and response time, while chip-level photoelectric sensors based on the thermo-optic effect can improve measurement sensitivity and reduce costs. This paper presents on-chip temperature sensors based on polysilicon (p-Si) waveguides. Dual-microring resonator (MRR) and asymmetric Mach–Zehnder interferometer (AMZI) sensors are demonstrated. The experimental results show that the sensitivities of the sensors based on AMZI and MRR are 86.6 pm/K and 85.7 pm/K, respectively. The temperature sensors proposed in this paper are compatible with the complementary metal-oxide-semiconductor (CMOS) fabrication technique. Benefitting from high sensitivity and a compact footprint, these sensors show great potential in the field of photonic-electronic applications.

Keywords: temperature sensors; polysilicon; dual-microring resonator; AMZI

Citation: Xu, X.; Yin, Y.; Sun, C.; Li, L.; Lin, H.; Tang, B.; Zhang, P.; Chen, C.; Zhang, D. Optical Temperature Sensor Based on Polysilicon Waveguides. *Sensors* **2022**, *22*, 9357. https://doi.org/10.3390/s22239357

Academic Editors: Vittorio M.N. Passaro and Francesco De Leonardis

Received: 14 November 2022
Accepted: 30 November 2022
Published: 1 December 2022

1. Introduction

Silicon photonics are a promising solution for large-scale and high-performance photonic integrated circuits (PICs) with a growing amount of applications in the optical interconnections [1,2], programmable photonics processors [3,4], and optical sensors [5–7]. Integrated silicon photonics sensors especially, have attracted great attention in the fields of environmental monitoring [8], industrial production [6,9], medical diagnosis [10], and chemical analysis [11], due to their high sensitivity, compact footprint, and mass production capabilities [12,13]. Besides high-performance optical sensors, readout equipment and interrogators are also crucial for lab-on-chip (LoC) photonic sensors [5,7].

Nowadays, most silicon photonic devices and circuits are demonstrated on the silicon-on-insulator (SOI) platform [14–16]. Crystalline silicon (c-Si) is the most widely used material due to its low optical losses and excellent electronic properties [17]. However, it is challenging to achieve three-dimensional (3D) multilayer PICs and electronic-photonics integrated circuits (EPICs) based on c-Si due to the extreme difficulty in full wafer bonding and polishing. In that case, low-temperature deposited materials such as hydrogenated amorphous silicon (a-Si:H) [18,19], silicon nitride (SiN) [20–25], or polysilicon (p-Si) [26] have been deposited and pattern above SOI wafers for multilayer PICs and EPICs. However, the low charge mobility in a-Si:H and SiN thin films limits their use as active components such as electro-optic modulators. P-Si, a collection of single-crystal silicon grains separated by grain boundaries, shows relatively low-loss and similar mobility to c-Si [27]. Additionally, the p-Si thin film transistor (TFT) has the merits such as high field effect mobility, high integration and high speed, high-definition display, low power consumption, and self-aligned structures [28–30]. With these good characteristics, p-Si is a promising material

for realizing multilayer active photonic devices and EPICs [31,32]. For a reliable on-chip system, a temperature monitor is necessary. Optical sensors have attracted lots of attention because of their high sensitivity, compact footprint, and property of anti-electromagnetic interference. To improve the reliability and performance of 3D PICs, in this paper, we demonstrate two kinds of p-Si temperature sensors based on the dual-microring resonator (MRR) and asymmetric Mach–Zehnder interferometer (AMZI). The temperature sensitivities of the sensors are 87 pm/K and 85 pm/K, respectively. Both of these sensors are suitable for temperature measurement of 3D PICs and EPICs.

2. Design, Fabrication, and Characterization

The devices were fabricated with the 180 nm p-Si photonic multi-project-wafer (MPW) process at the Institute of Microelectronics of the Chinese Academy of Sciences (IMECAS). The 220 nm thick p-Si was deposited on the SiO_2 buffer at 2 µm of thickness at 620 °C. The sensor is designed for C-band operation. For single-mode propagation, the geometry of the waveguide is 500 nm × 220 nm. Deep ultraviolet (DUV) photolithography was employed to define the waveguide patterns, followed by inductively coupled plasma (ICP) etching of silicon. To simplify the fabrication process, we chose one-step etching of 150 nm for both grating couplers and ridge waveguides. A 1 µm thick SiO_2 upper cladding was deposited on the waveguides.

2.1. The Structure of MRR

MRRs are usually compact with a typical radius of several micrometers. The narrow linewidth of resonance dip is attractive for highly sensitive optical sensors [33]. However, the large detection range means a small ring radius, which results in increased bending loss in the ring. To overcome the trade-off between detection range and sensitivity, we adopt a dual-MRR structure with different circumferences and a different free spectral range (FSR), as shown in Figure 1. As a result, the transmittance reaches the minimum only at the overlapped resonant peaks for each of the ring resonator.

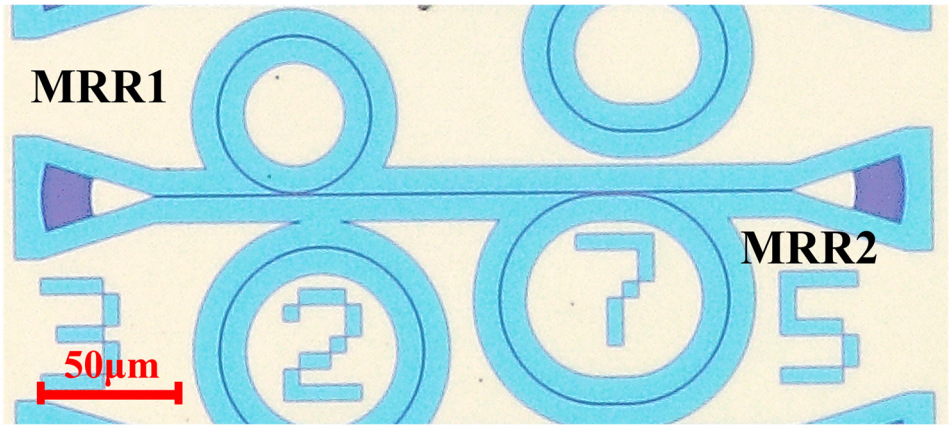

Figure 1. Microscopic image of the dual-MRR temperature sensor.

Our dual-MRR sensor consists of a ring (MRR1) and a racetrack (MRR2) resonator. The gap between the ring and bus waveguide is 300 nm. The racetrack resonator consists of a directional coupling (DC) coupling region. For the coupling region, the gap and the length are 400 nm and 10 µm, respectively. The radii of the ring and racetrack are 30 µm and 40 µm, respectively. A broadband tunable laser system (Santec Full-band TSL-550) covering the ultra-wide tuning range of 1260 nm to 1630 nm was used to characterize the fabricated devices. The resolution is 1 pm for MRR, narrow linewidth components, in the measurements. This system combines up to three tunable lasers (TSL-550) with an optical switch module (OSA-110). The light from output grating is measured through an optical power meter (MPM-210H). The light from laser and devices is coupled into the devices through a vertical fiber coupling system with a polarization controller. The

minimum loss of the reference grating is ~10.42 dB for the fundamental transverse electric (TE) mode. The spectrum of the dual-MRR sensor from 1543 nm to 1568 nm at 25 °C is shown in Figure 2a. The on-chip insertion loss is ~1.46 dB. Two group resonances with different FSRs are observed. The FSRs for different MRRs are FSR1 = 2.9 nm and FSR2 = 2.41 nm, respectively. We observe the resonance dips at 1546.00 nm and 1578 nm. The FSR for our dual-MRR is about 14.56 nm. Figure 2b shows the transmission of the resonator peak at 1560.56 nm. The full width at half maximum (FWHM) of the resonance peak for the present resonator is about $\Delta\lambda$ = 463 pm at 1560.56 nm, indicating a loaded Q factor $Q_{load} = \lambda/\Delta\lambda$ of 3370.

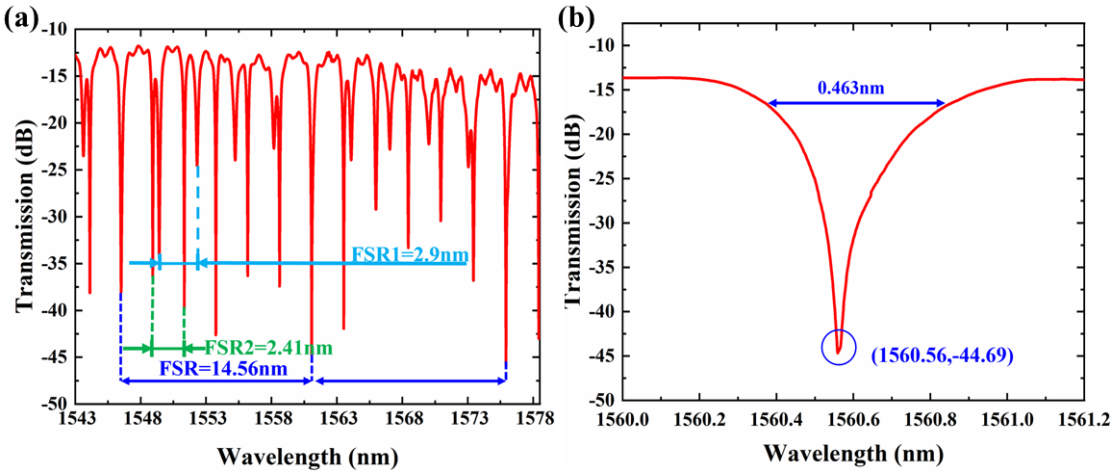

Figure 2. (**a**) The spectrum of the dual-MRR sensor. (**b**) The transmission of overlapping resonant peaks.

The temperature response of the sensor was investigated by placing it on a high-precision temperature console stage with a temperature resolution of 0.1 K. Figure 3a shows the measured spectra of the dual-MRR temperature sensor, indicating a linear wavelength shift with temperature from 0 K to 20 K. The resonant wavelength is extracted and linearly fitted as shown in Figure 3b. The slope of fitting results presents the temperature sensitivity, which is calculated as $\Delta\lambda/\Delta T$ = 85.74 pm/K with a correlation coefficient (R^2) of 0.99996.

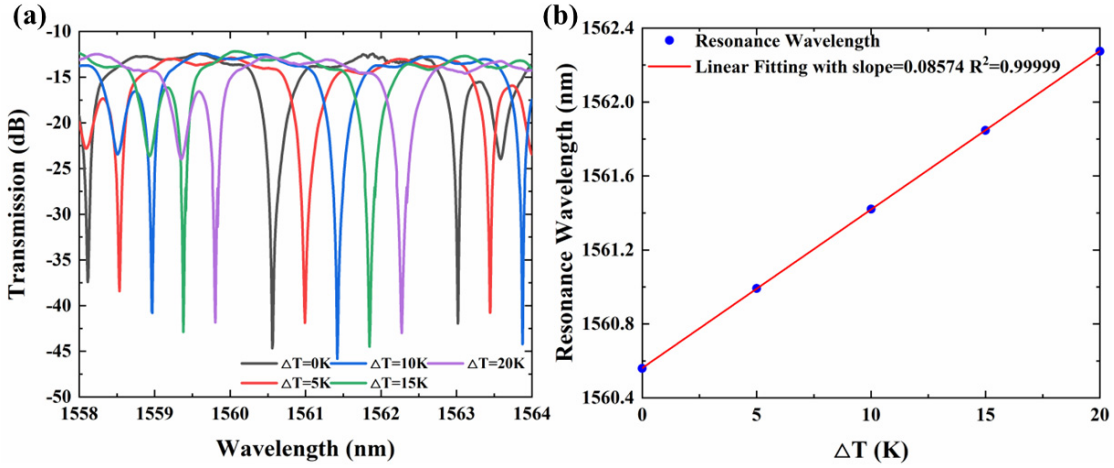

Figure 3. (**a**) Spectra of the dual-MRR sensor at different temperatures (ranging from 0 K to 20 K). (**b**) Overlapping resonant peak wavelength at different temperatures.

2.2. The Structure of AMZI

Mach–Zehnder Interferometers (MZIs), one of the most widely used structures, have been demonstrated in a wide range of applications, including wavelength division multiplexers [34,35], optical switches [36], electro-optical modulators [37] and biosensors [38,39].

In this paper, we also propose AMZI temperature sensors based on the p-Si platform. The microscopic image of AMZI is shown in Figure 4. It consists of two 3 dB couplers and two arms with different lengths. Directional coupler (DC), Y-branch splitter, and multi-mode interferences (MMI) are common structures for 3 dB couplers. Considering with the bandwidth and process tolerance, we choose MMI as 3 dB couplers for the AMZI sensors.

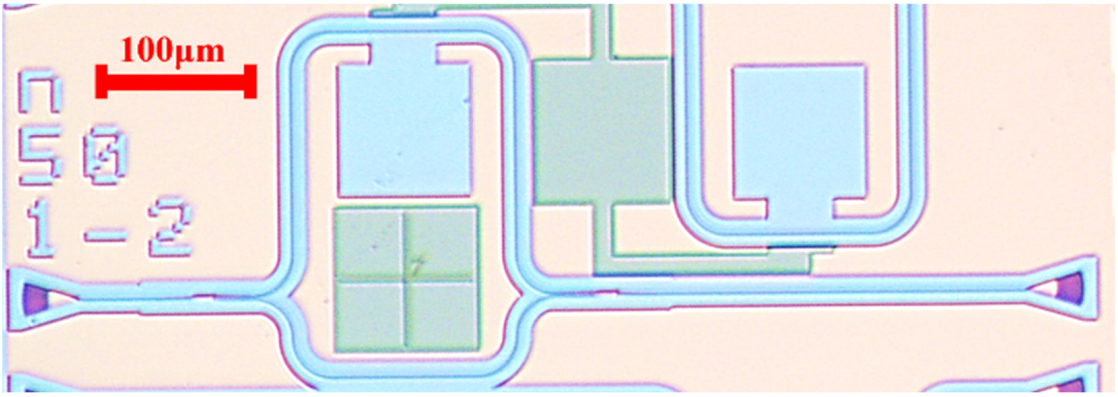

Figure 4. Microscopic image of the temperature sensor based on AMZI.

The 1 × 2 MMI used in the sensor is shown in Figure 5a. A series of cascaded MMIs were fabricated to characterize the insertion loss and uniformity of the output waveguides, as shown in Figure 5b. Transmission spectra from ports 1–7 in the range of 1460 nm to 1580 nm are shown in Figure 5c. Then, we fit the transmission loss at 1550 nm and found the slope of the linear fitting was −4.45, as shown in Figure 5d. It means the excess loss of MMI is 1.54 dB. The MMI shows superior uniformity according to the transmission spectra of ports 6 and 7.

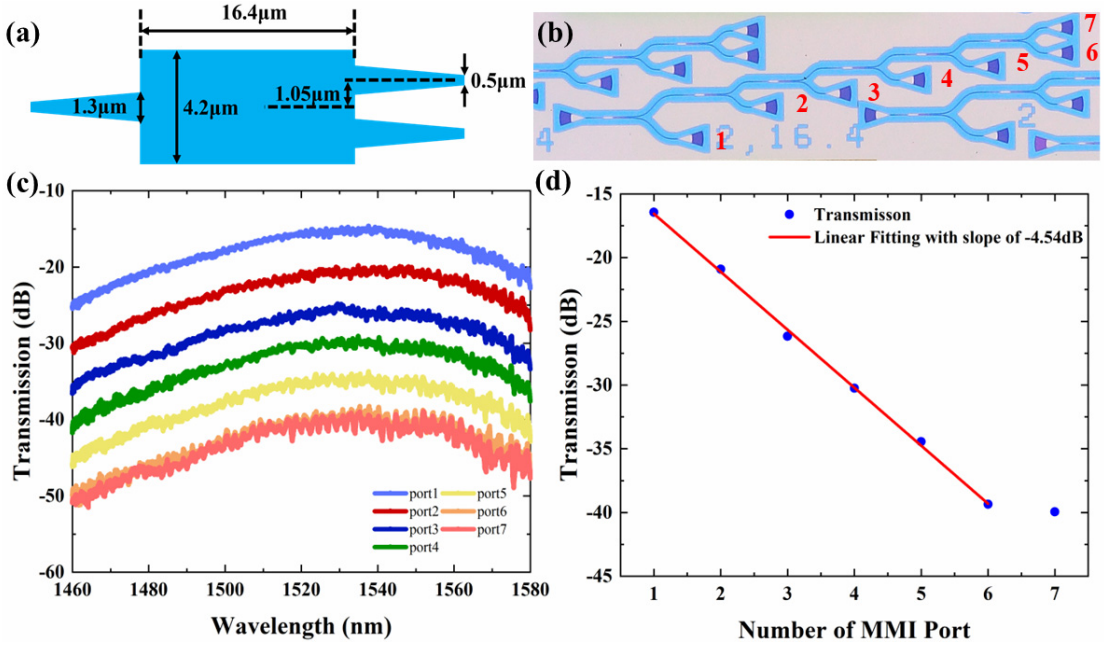

Figure 5. (**a**) Schematic of 1 × 2 MMI. (**b**) Microscopic image of the cascade MMI. (**c**) Measured trans-mission spectra of the cascaded 1 × 2 MMIs at the wavelength range of 1460–1580 nm. (**d**) Linear fitting of the normalized transmission at 1550 nm wavelength.

The FSR is also important for an AMZI, which is given by

$$FSR = \frac{\lambda^2}{n_g \Delta L} \quad (1)$$

where λ is the center wavelength, n_g is the group index, and ΔL is the path length difference between the arms. The group index n_g is 4.11, which is calculated through finite difference eigenmode (FDE) method. The center wavelength λ is 1550 nm. The interferometer path length difference ΔL is 280 μm. Thus, the FSR of AMZI is 2.08 nm.

The same characterization system with a dual-MRR sensor is applied for the AMZI. The transmission spectrum of our designed AMZI sensor is shown in Figure 6 when the temperature is 25 °C. The AMZI shows an insertion of 16.5 dB. The FSR of AMZI is 2.06 nm, which is consistent with the calculated result.

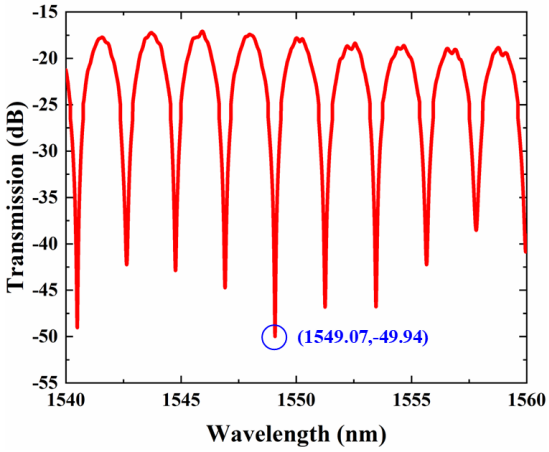

Figure 6. The spectrum of our designed AMZI.

We chose the resonant wavelength dip at 1549.07 nm to demonstrate the sensing application. The drift of the characteristic wavelength observes the temperature change. Figure 7a plots the spectrum change of AMZI when the temperature change varies from 0 K to 20 K. The extinction ratios of our designed AMZI's resonant peak are almost constant with increasing temperatures. Figure 7b shows the linear fitting of the resonant wavelength changing with temperature changing. The sensitivity of the temperature sensor, which equals the slope of the straight line, is 0.0866 with a correlation coefficient (R^2) of 0.998. Therefore, the AMZI sensor has a sensitivity of 86.66 pm/K.

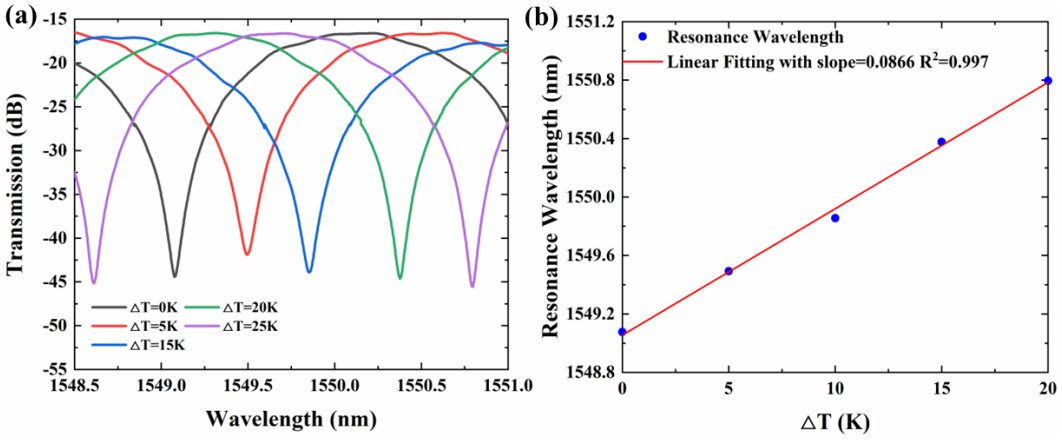

Figure 7. (**a**) Spectra of the AMZI sensor at different ambient temperatures. (**b**) Resonant peak wave-length at different temperatures and linear fitting.

3. Discussion

The performance comparison between temperature sensors on different platforms is listed in Table 1. In [40], a silicon-based dual-polarization MRR with a polyvinyl-alcohol (PVA) upper cladding is demonstrated for measuring humidity and temperature simultaneously. For TE and transverse magnetic (TM) polarization modes, the sensitivities of the sensor are 69.0 pm/K and 30.6 pm/K, respectively. Multifunctional sensors with humidity and temperature monitors are attractive, but sensitivity is lower than in our work. Low depth for the TM mode resonator is also a challenge for practical applications. To increase the sensitivity, fano resonance is achieved by introducing an air hole with a diameter of 368 µm into the center of the coupling [41]. However, the sensitivity is only 75.3 pm/K with an extinction ratio (ER) of 9.57 dB. Both of the MRR- and AMZI-based sensors demonstrated in this paper show a large ER of ~35 dB. However, the gap between the bus waveguide and ring of the sensor in [41] is 83 nm, which is hard for a MPW process. Replacing the silicon or silica waveguides with polymer waveguides is another effective method to improve the sensitivity. In [42], a MZI sensor with two arms consisting of hybrid waveguides providing the opposite temperature-dependent phase changes is demonstrated. One arm of the MZI sensor is narrowed to 40 nm, leaking the light to SU-8 cladding with a negative thermal optical coefficient (TOC). The opposite temperature dependent phase change enhances the sensitivity to 172 pm/K. In [43], a chip-scale temperature sensor with a high sensitivity of 228.6 pm/K based on a rhodamine 6G (R6G)-doped SU-8 whispering gallery mode microring laser is developed. However, polymer materials need an effective method to improve their long-term stability [44,45]. Using the same whispering gallery mode microring structure, a low sensitivity of 19.37 pm/K is measured, owing to low TOC of SiN [46]. Another effective method is using Michelson interferometer (MI) to improve the influence of light propagation by heater. A compact size of 120 µm × 80 µm temperature sensors with 113.7 pm/k sensitivity is achieved [47]. This structure is also useful for thermo-optic switches [48]. In our work, we demonstrate two types p-Si temperature sensors based on MRR and AMZI structures. The fabrication is well compatible with the CMOS fabrication technique. Low fabrication temperatures enable the p-Si sensor to be used in multilayer integrated optical circuits. The sensitivity is to the same degree as the c-Si sensor. With new material introduced and useful structure applied, the sensitivity could be improved sharply. Moreover, p-Si is a normal material for electronic integrated circuits. A fully integrated biosensing electronic–photonic system-on-chip (EPSoC) could be achieved using this platform [7,49,50].

Table 1. Comparison of temperature senors.

Reference	Waveguide Materails	Structure	Sensitivity (pm/K)	Radius/Footprint
[40]	c-Si	MRR	69.0 pm/K	20 µm
[41]	c-Si	MRR	75.3 pm/K	20 µm
[42]	c-Si	AMZI	172 pm/K	N.A.
[43]	R6G-SU-8	MRR	228.6 pm/K	110 µm
[46]	SiN	MRR	19.37 pm/K	100 µm
[47]	c-Si	MI	113.7 pm/K	120 µm × 80 µm
This work	p-Si	MRR	85.7 pm/K	30 µm
This work	p-Si	AMZI	86.6 pm/K	400 µm × 260 µm

4. Conclusions

In conclusion, we demonstrated two types of p-Si temperature sensors experimentally. The two types of sensors were dual-MRR and AMZI structures. The dual-MRR sensor had a large FSR of 14.56 nm and the Q_{load} of dual-MRR is 3370. We optimized the 1 × 2 MMI of the AMZI sensor with an excess loss of 1.54 dB and uniform spectral uniformity. For both sensors, we used the shift of the resonant wavelengths to calculate the amount of temperature change. The results show the sensitivity of the dual-MRR sensor and AMZI

sensor are 85.74 pm/K and 86.6 pm/K, respectively. It confirms that the temperature sensors based on the p-Si waveguides have large temperature sensitivity and a compact footprint. Therefore, they show great potential to realize temperature monitoring of multilayer integrated optical circuits and EPICs.

Author Contributions: Conceptualization, X.X. and Y.Y.; methodology, X.X.; software, X.X.; validation, X.X., Y.Y. and D.Z.; formal analysis, X.X.; investigation, X.X.; resources, C.S., P.Z. and B.T.; data curation, X.X.; writing—original draft preparation, X.X.; writing—review and editing, Y.Y.; visualization, X.X.; supervision, L.L., H.L. and C.C.; project administration, L.L., H.L. and D.Z.; funding acquisition, L.L., H.L. and D.Z. All authors have read and agreed to the published version of the manuscript.

Funding: This work was funded by the National Key Research and Development Program of China (No. 2019YFB2203003).

Institutional Review Board Statement: Not applicable.

Informed Consent Statement: Not applicable.

Data Availability Statement: Not applicable.

Conflicts of Interest: The authors declare no conflict of interest.

References

1. Lee, B.G.; Dupuis, N. Silicon Photonic Switch Fabrics: Technology and Architecture. *J. Lightwave Technol.* **2019**, *37*, 6–20. [CrossRef]
2. Suzuki, K.; Konoike, R.; Suda, S.; Matsuura, H.; Namiki, S.; Kawashima, H.; Ikeda, K. Low-Loss, Low-Crosstalk, and Large-Scale Optical Switch Based on Silicon Photonics. *J. Lightwave Technol.* **2020**, *38*, 233–239. [CrossRef]
3. Zand, I.; Bogaerts, W. Effects of coupling and phase imperfections in programmable photonic hexagonal waveguide meshes. *Photonics Res.* **2020**, *8*, 211–218. [CrossRef]
4. Bogaerts, W.; Chen, X.; Deng, H.; Van Iseghem, L.; Wang, M.; Zand, I.; Zhang, Y.; Liu, Y.; Nagarjun, K.P.; Khan, U. Programmable Silicon Photonic Circuits. In Proceedings of the 2022 27th OptoElectronics and Communications Conference (OECC) and 2022 International Conference on Photonics in Switching and Computing (PSC), Toyama, Japan, 3–6 July 2022; pp. 1–3.
5. Yang, F.; Zhang, W.; Jiang, Y.; Tao, J.; He, Z. Highly Sensitive Integrated Photonic Sensor and Interrogator Using Cascaded Silicon Microring Resonators. *J. Lightwave Technol.* **2022**, *40*, 3055–3061. [CrossRef]
6. Luo, M.; Yang, Q.; Dong, F.; Chen, N.; Liao, W. Miniature Micro-Ring Resonator Sensor With Electro-Optic Polymer Cladding for Wide-Band Electric Field Measurement. *J. Lightwave Technol.* **2022**, *40*, 2577–2584. [CrossRef]
7. Adamopoulos, C.; Buchbinder, S.; Zarkos, P.; Bhargava, P.; Gharia, A.; Niknejad, A.; Anwar, M.; Stojanovic, V. Fully Integrated Electronic–Photonic Biosensor for Label-Free Real-Time Molecular Sensing in Advanced Zero-Change CMOS-SOI Process. *IEEE Solid-State Circuits Lett.* **2021**, *4*, 198–201. [CrossRef]
8. Yu, H.; Sun, X.; Liu, G.; Fateh, U.; Ban, D.; Deng, N.; Qiu, F. Gas environment independent temperature sensor via double-metal surface plasmon resonance. *Opt. Express* **2021**, *29*, 15393–15402. [CrossRef] [PubMed]
9. Ou, X.; Yang, Y.; Sun, F.; Zhang, P.; Tang, B.; Li, B.; Liu, R.; Liu, D.; Li, Z. Wide-range, ultra-compact, and high-sensitivity ring resonator biochemical sensor with CMOS-compatible hybrid plasmonic waveguide. *Opt. Express* **2021**, *29*, 19058–19067. [CrossRef]
10. Kohler, D.; Schindler, G.; Hahn, L.; Milvich, J.; Hofmann, A.; Lange, K.; Freude, W.; Koos, C. Biophotonic sensors with integrated Si3N4-organic hybrid (SiNOH) lasers for point-of-care diagnostics. *Light Sci. Appl.* **2021**, *10*, 64. [CrossRef]
11. Tao, J.; Wang, X.; Sun, T.; Cai, H.; Wang, Y.; Lin, T.; Fu, D.; Ting, L.L.; Gu, Y.; Zhao, D. Hybrid Photonic Cavity with Metal-Organic Framework Coatings for the Ultra-Sensitive Detection of Volatile Organic Compounds with High Immunity to Humidity. *Sci. Rep.* **2017**, *7*, 41640. [CrossRef]
12. Nazemi, H.; Joseph, A.; Park, J.; Emadi, A. Advanced Micro- and Nano-Gas Sensor Technology: A Review. *Sensors* **2019**, *19*, 1285. [CrossRef]
13. Fernandez Gavela, A.; Grajales Garcia, D.; Ramirez, J.C.; Lechuga, L.M. Last Advances in Silicon-Based Optical Biosensors. *Sensors* **2016**, *16*, 285. [CrossRef] [PubMed]
14. Chen, W.; Wang, W.; Guo, W.; Gong, Z.; Zhou, H.; Zhou, Q.; Jiang, X.; Yang, J. A 2 x 2 nonblocking Mach-Zehnder-based silicon switch matrix. *Opt. Express* **2012**, *20*, 12593–12598. [CrossRef]
15. Juhari, N.; Menon, P.S.; Ehsan, A.A. 12-channel tapered SOI-based AWG for CWDM system. In Proceedings of the 2013 IEEE 4th International Conference on Photonics (ICP), Melaka, Malaysia, 28–30 October 2013; pp. 230–233.
16. de Cea, M.; Fini, J.; Van Orden, D.; Wade, M.; Stojanovic, V.; Ram, R.J. 18 GHz 3 dB bandwidth SiGe resonant photodetector in 45 nm SOI CMOS. In Proceedings of the 2020 IEEE Photonics Conference (IPC), Vancouver, BC, Canada, 28 September–1 October 2020; pp. 1–2.

17. Yang, Z.; Kwong, D.; Xiaochuan, X.; Hosseini, A.; Yang, S.Y.; Rogers, J.A.; Chen, R.T. Inter-layer grating coupler on double-layer silicon nanomembranes. In Proceedings of the 2013 Optical Interconnects Conference, Santa Fe, NM, USA, 5–8 May 2013; pp. 35–36.
18. JoonHyun, K.; Atsumi, Y.; Hayashi, Y.; Suzuki, J.; Kuno, Y.; Amemiya, T.; Nishiyama, N.; Arai, S. Amorphous-Silicon Inter-Layer Grating Couplers With Metal Mirrors Toward 3-D Interconnection. *IEEE J. Sel. Top. Quantum Electron.* **2014**, *20*, 317–322. [CrossRef]
19. Lacava, C.; Ettabib, M.A.; Cristiani, I.; Fedeli, J.M.; Richardson, D.J.; Petropoulos, P. Ultra-Compact Amorphous Silicon Waveguide for Wavelength Conversion. *IEEE Photonics Technol. Lett.* **2016**, *28*, 410–413. [CrossRef]
20. Shang, K.; Pathak, S.; Guan, B.; Liu, G.; Yoo, S.J. Low-loss compact multilayer silicon nitride platform for 3D photonic integrated circuits. *Opt. Express* **2015**, *23*, 21334–21342. [CrossRef] [PubMed]
21. Suzuki, K.; Namiki, S.; Kawashima, H.; Ikeda, K.; Konoike, R.; Yokoyama, N.; Seki, M.; Ohtsuka, M.; Saitoh, S.; Suda, S.; et al. Nonduplicate Polarization-Diversity 32 × 32 Silicon Photonics Switch Based on a SiN/Si Double-Layer Platform. *J. Lightwave Technol.* **2020**, *38*, 226–232. [CrossRef]
22. Konoike, R.; Suzuki, K.; Tanizawa, K.; Suda, S.; Matsuura, H.; Namiki, S.; Kawashima, H.; Ikeda, K. SiN/Si double-layer platform for ultralow-crosstalk multiport optical switches. *Opt. Express* **2019**, *27*, 21130–21141. [CrossRef]
23. Zhang, L.; Li, Y.; Chen, B.; Wang, Y.; Li, H.; Hou, Y.; Tao, M.; Li, Y.; Zhi, Z.; Liu, X.; et al. Two-dimensional multi-layered SiN-on-SOI optical phased array with wide-scanning and long-distance ranging. *Opt. Express* **2022**, *30*, 5008–5018. [CrossRef]
24. Wang, P.; Luo, G.; Xu, Y.; Li, Y.; Su, Y.; Ma, J.; Wang, R.; Yang, Z.; Zhou, X.; Zhang, Y.; et al. Design and fabrication of a SiN-Si dual-layer optical phased array chip. *Photonics Res.* **2020**, *8*, 912–919. [CrossRef]
25. Siew, S.Y.; Li, B.; Gao, F.; Zheng, H.Y.; Zhang, W.; Guo, P.; Xie, S.W.; Song, A.; Dong, B.; Luo, L.W.; et al. Review of Silicon Photonics Technology and Platform Development. *J. Lightwave Technol.* **2021**, *39*, 4374–4389. [CrossRef]
26. Preston, K.; Schmidt, B.; Lipson, M. Polysilicon photonic resonators for large-scale 3D integration of optical networks. *Opt. Express* **2007**, *15*, 17283–17290. [CrossRef]
27. Franz, Y.; Runge, A.F.J.; Oo, S.Z.; Jimenez-Martinez, G.; Healy, N.; Khokhar, A.; Tarazona, A.; Chong, H.M.H.; Mailis, S.; Peacock, A.C. Laser crystallized low-loss polycrystalline silicon waveguides. *Opt. Express* **2019**, *27*, 4462–4470. [CrossRef]
28. Song, I.-H.; Han, M.-K. Low temperature poly-Si TFTs for display application. *Curr. Appl. Phys.* **2003**, *3*, 363–366. [CrossRef]
29. Wang, L.; Sun, L.; Han, D.; Wang, Y.; Chan, M.; Zhang, S. A Hybrid a-Si and Poly-Si TFTs Technology for AMOLED Pixel Circuits. *J. Disp. Technol.* **2014**, *10*, 317–320. [CrossRef]
30. Shen-De, W.; Wei-Hsiang, L.; Tzu-Yun, C.; Tan-Fu, L. A novel process-compatible fluorination technique with electrical characteristic improvements of poly-Si TFTs. *IEEE Electron Device Lett.* **2005**, *26*, 372–374. [CrossRef]
31. Stojanovic, V.; Ram, R.J.; Popovic, M.; Lin, S.; Moazeni, S.; Wade, M.; Sun, C.; Alloatti, L.; Atabaki, A.; Pavanello, F.; et al. Monolithic silicon-photonic platforms in state-of-the-art CMOS SOI processes [Invited]. *Opt. Express* **2018**, *26*, 13106–13121. [CrossRef] [PubMed]
32. Hung, Y.J.; Tang, C.T.; Chen, T.H.; Yen, T.H.; Tsai, M.J.; Lee, S.L. Low-loss polysilicon subwavelength grating waveguides and narrowband Bragg reflectors in bulk CMOS. *Opt. Express* **2020**, *28*, 7786–7798. [CrossRef] [PubMed]
33. Kim, H.-T.; Yu, M. Cascaded ring resonator-based temperature sensor with simultaneously enhanced sensitivity and range. *Opt. Express* **2016**, *24*, 9501–9510. [CrossRef]
34. Yen, T.-H.; Hung, Y., Jr. Fabrication-Tolerant CWDM (de)Multiplexer Based on Cascaded Mach–Zehnder Interferometers on Silicon-on-Insulator. *J. Lightwave Technol.* **2021**, *39*, 146–153. [CrossRef]
35. Xu, H.; Shi, Y. Flat-Top CWDM (De)Multiplexer Based on MZI With Bent Directional Couplers. *IEEE Photonics Technol. Lett.* **2018**, *30*, 169–172. [CrossRef]
36. Qiao, L.; Tang, W.; Chu, T. 32 × 32 silicon electro-optic switch with built-in monitors and balanced-status units. *Sci. Rep.* **2017**, *7*, 42306. [CrossRef]
37. Palmer, R.; Alloatti, L.; Korn, D.; Schindler, P.C.; Baier, M.; Bolten, J.; Wahlbrink, T.; Waldow, M.; Dinu, R.; Freude, W.; et al. Low Power Mach–Zehnder Modulator in Silicon-Organic Hybrid Technology. *IEEE Photonics Technol. Lett.* **2013**, *25*, 1226–1229. [CrossRef]
38. Qin, K.; Hu, S.; Retterer, S.T.; Kravchenko, I.I.; Weiss, S.M. Slow light Mach-Zehnder interferometer as label-free biosensor with scalable sensitivity. *Opt. Lett.* **2016**, *41*, 753–756. [CrossRef] [PubMed]
39. Goodwin, M.J.; Besselink, G.A.J.; Falke, F.; Everhardt, A.S.; Cornelissen, J.J.L.M.; Huskens, J. Highly Sensitive Protein Detection by Asymmetric Mach–Zehnder Interferometry for Biosensing Applications. *ACS Appl. Bio. Mater.* **2020**, *3*, 4566–4572. [CrossRef] [PubMed]
40. Ding, Z.; Liu, P.; Chen, J.; Dai, D.; Shi, Y. On-chip simultaneous sensing of humidity and temperature with a dual-polarization silicon microring resonator. *Opt. Express* **2019**, *27*, 28649–28659. [CrossRef]
41. Zhang, C.; Kang, G.; Xiong, Y.; Xu, T.; Gu, L.; Gan, X.; Pan, Y.; Qu, J. Photonic thermometer with a sub-millikelvin resolution and broad temperature range by waveguide-microring Fano resonance. *Opt. Express* **2020**, *28*, 12599–12608. [CrossRef]
42. Guan, X.; Wang, X.; Frandsen, L.H. Optical temperature sensor with enhanced sensitivity by employing hybrid waveguides in a silicon Mach-Zehnder interferometer. *Opt. Express* **2016**, *24*, 16349–16356. [CrossRef]
43. Wan, L.; Chandrahalim, H.; Chen, C.; Chen, Q.; Mei, T.; Oki, Y.; Nishimura, N.; Guo, L.J.; Fan, X. On-chip, high-sensitivity temperature sensors based on dye-doped solid-state polymer microring lasers. *Appl. Phys. Lett.* **2017**, *111*, 061109. [CrossRef]

44. Noh, Y.-O.; Lee, C.-H.; Kim, J.-M.; Hwang, W.-Y.; Won, Y.-H.; Lee, H.-J.; Han, S.-G.; Oh, M.-C. Polymer waveguide variable optical attenuator and its reliability. *Opt. Commun.* **2004**, *242*, 533–540. [CrossRef]
45. Lu, G.W.; Hong, J.; Qiu, F.; Spring, A.M.; Kashino, T.; Oshima, J.; Ozawa, M.A.; Nawata, H.; Yokoyama, S. High-temperature-resistant silicon-polymer hybrid modulator operating at up to 200 Gbit s(-1) for energy-efficient datacentres and harsh-environment applications. *Nat. Commun.* **2020**, *11*, 4224. [CrossRef] [PubMed]
46. Zhang, C.; Kang, G.-G.; Wang, J.; Wan, S.; Dong, C.-H.; Pan, Y.-J.; Qu, J.-F. Photonic thermometer by silicon nitride microring resonator with milli-kelvin self-heating effect. *Measurement* **2022**, *188*, 110494. [CrossRef]
47. Tao, J.F.; Cai, H.; Gu, Y.D.; Wu, J.; Liu, A.Q. Demonstration of a Photonic-Based Linear Temperature Sensor. *IEEE Photonics Technol. Lett.* **2015**, *27*, 767–769. [CrossRef]
48. Zeqin, L.; Murray, K.; Jayatilleka, H.; Chrostowski, L. Michelson Interferometer Thermo-Optic Switch on SOI With a 50-μW Power Consumption. *IEEE Photonics Technol. Lett.* **2015**, *27*, 2319–2322. [CrossRef]
49. Sun, C.; Wade, M.T.; Lee, Y.; Orcutt, J.S.; Alloatti, L.; Georgas, M.S.; Waterman, A.S.; Shainline, J.M.; Avizienis, R.R.; Lin, S.; et al. Single-chip microprocessor that communicates directly using light. *Nature* **2015**, *528*, 534–538. [CrossRef]
50. Atabaki, A.H.; Moazeni, S.; Pavanello, F.; Gevorgyan, H.; Notaros, J.; Alloatti, L.; Wade, M.T.; Sun, C.; Kruger, S.A.; Meng, H.; et al. Integrating photonics with silicon nanoelectronics for the next generation of systems on a chip. *Nature* **2018**, *556*, 349–354. [CrossRef]